IEEE Access
Multidisciplinary | Rapid Review | Open Access Journal

Received October 25, 2016; accepted December 2, 2016, date of publication December 8, 2016, date of current version January 4, 2017.

*Digital Object Identifier 10.1109/ACCESS.2016.2637822*

# Linear State Feedback Regulation of a Furuta Pendulum: Design Based on Differential Flatness and Root Locus

**VICTOR MANUEL HERNÁNDEZ-GUZMÁN[1], MAYRA ANTONIO-CRUZ[2], AND RAMÓN SILVA-ORTIGOZA[2]**

[1]Facultad de Ingeniería, Universidad Autónoma de Querétaro, Querétaro 76150, Mexico
[2]Instituto Politécnico Nacional, CIDETEC, Área de Mecatrónica, México City 07700, Mexico

Corresponding author: V. M. Hernández-Guzmán (vmhg@uaq.mx)

The work of V. M. Hernández-Guzmán was supported by SNI-México. The Work of M. Antonio-Cruz was supported by CONACYT-México and BEIFI-IPN scholarships. The work of R. Silva-Ortigoza was supported by SNI-México and IPN Programs EDI and COFAA.

**ABSTRACT** Different educational and didactic papers that allow students to experimentally validate linear controllers have been reported. However, generally, in those papers, procedure followed to select controller gains is not discussed. This lack of information renders difficult experimental implementation of controllers by students who, in general, do not have enough experience on controller tuning. Motivated by this situation, this paper introduces a methodology that provides important information on how to select controller gains for regulation in a Furuta pendulum. This methodology allows improving closed-loop system performance in a desired direction. Differential flatness is the Furuta pendulum property that is exploited. The main idea is to translate a linear state feedback control design problem into a scenario, where classical tools such as root locus can be used. As an example, controller design is directed toward reduction or even elimination of limit cycle effects. The proposal is experimentally tested on a built Furuta pendulum. These experimental results show that the closed-loop system performance is improved, and hence, the proposed methodology is successfully validated.

**INDEX TERMS** Automatic control education, classical control, root locus, differential flatness, state feedback control, gain selection, furuta pendulum, stabilization.

## I. INTRODUCTION

Automatic control is an important subject taught in many engineering majors such as electrical engineering, electronics, bionics, robotics, mechatronics, etc. However, the complex mathematical and abstract concepts treated in this subject result difficult to understand and grasp for most students. To solve this, different pedagogical and didactic materials allowing the students to experimentally validate automatic control theory have been developed by educators and researchers at different engineering areas and levels (undergraduate, graduate, and postgraduate) [1]–[8]. Various systems have been used for such an aim [9]–[16], among them inverted pendulums are found due to their simple configuration, nonlinearity, underactuation, etc.

Educational work related to the control of inverted pendulums is as follows. Giron-Sierra [17] presented the description of an inverted pendulum actuated by two electromagnets. A program based on MS-DOS and Borland C++ was developed by students to stabilize such a pendulum. Sánchez *et al*. [18] introduced a web-based laboratory, which allows the remote control of an inverted pendulum on a car. To stabilize the pendulum an LQR controller was designed. Rodriguez *et al*. [19] developed an environment for the modeling, simulation, animation, and real-time control of electromechanical cart-pendulums. This environment was based on Microsoft Windows, Visual C++, Direct-3D, and MATLAB/Simulink. Furthermore, Petrić and Šitum [20], considering a pneumatic actuation, built three underactated systems: the inverted pendulum on a cart, the inverted wedge, and the ball and beam. Also, they implemented a state-variable feedback with LQR optimal design for the three systems. Additionally, this control with an observer was applied to the inverted wedge and a cascade compensation was implemented in the ball and beam. Lee *et al*. [21], [22]

reported an educational kit intended to the intelligent control system education. This kit included an inverted pendulum on a cart, the control hardware, and a graphical user interface. Using this kit a PID, an FEL scheme, an RTC scheme, and an adaptive neuro-fuzzy controller were implemented to execute balancing and tracking control. Moreover, Lin and Tsai [23] developed and controlled a human transportation vehicle for teaching automatic control theory in undergraduate engineering areas. For this, an education process and a pedagogical method were presented. Stefanovic *et al*. [24] reported a web-based laboratory for the remote control of an inverted pendulum and a crane system. This with the intention of teaching control concepts by means of experiments through the internet at any time and from any location. Mahmoodabadi *et al*. [25] introduced a multi-objective particle swarm optimization method for the tuning of the state feedback control gain vector. This method was applied to the inverted pendulum and ball and beam. The simulations were carried out with Java applets. By they part, Zhou *et al*. [26] presented a practice-oriented intuitive approach, in which the students were motivated to construct and control an inverted pendulum on a car based on their intuition. Demirtas *et al*. [27] reported a virtual laboratory based on LabVIEW for graduate students, which included sliding mode and PID control for the Furuta pendulum. There, the parameters of the system and the controls could be modified. Quian *et al*. [28] introduced a control based on energy to set the deviation of an inverted pendulum on a car. This in the direction of stabilizing the system through a state-feedback control optimized by the LQR algorithm. The validation of the approach was carried out by students through experiments. Recently, Canale and Casale-Brunet [29] used a wheeled inverted pendulum, derived from the Lego Mindstorms NXT, for theoretical and practical teaching of model predictive control. The designed control for the system was described step-by-step and experimentally implemented. Lin *et al*. [30] developed an inertia flywheel pendulum mechatronic kit that includes a hybrid controller, integrated by an energy control and a genetic algorithm PID control for swinging-up and stabilizing the pendulum, respectively. The intention of this mechatronic kit was to teach control courses to university students. Other educational papers related to automatic control theory, such as modeling [31], construction [32], [33], and linearization [34] of inverted pendulums have been reported. Particularly, the Furuta pendulum is a suitable prototype for education because it has two-degrees-of-freedom, it is underactuated, complex enough to exhibit interesting phenomena but it is not difficult to built using low cost materials and to control using hardware that is well known by students. Several research works have been presented for the Furuta pendulum solving the swing-up [35]–[38], stabilization [39]–[41], hybrid control [42]–[44], trajectory tracking [45]–[47], and oscillation shaping [48]–[50].

Having reviewed the related work it was found that, generally, a satisfactory control implementation in inverted pendulums is included. However, few papers describe the procedure followed for the controller gain selection. For such an aim, the trial and error approach is the one commonly used. However, it is difficult for students since several sets of gains have to be chosen and tested until a desired system performance be obtained. Furthermore, all of this has to be accomplished without any information on how to modify controller gains to enhance performance in a particular direction. This discourages students to continue exploring automatic control topics. Motivated by this scenario, this paper introduces a methodology to select the gain vector of a linear state feedback controller that stabilizes the Furuta pendulum at the upright pendulum configuration. Such a methodology is focused on improving closed-loop system performance by reducing or even eliminating effects of limit cycles, which appear because of the dead zone induced by static friction at shaft of motor used as actuator. This methodology exploits the Furuta pendulum differential flatness property [51] to translate a linear state feedback control design problem into a design scenario where classical tools such as root locus can be employed. Advantages of this methodology are: i) it allows study of limit cycles when the pendulum is stabilized, ii) effects of limit cycles can be reduced or even eliminated, iii) students access to important information for controller gain selection, iv) it allows to practice and, in consequence, to strength classical and modern linear control theory discussed in the classroom, v) contrary to optimization techniques used for control tuning, such as genetic algorithms [25], [52] and fuzzy logic [53], [54], the proposed methodology exploits approaches commonly studied in basic automatic control courses.

The first hypothesis in this paper is that selecting controller gains for a linear state feedback controller can be accomplished using classical control techniques. However, application of classical control techniques requires a transfer function which needs definition of a system output. Hence, one design problem is the selection of the system output for the Furuta pendulum, since there are two important variables to control: pendulum position and arm position. In this respect, several results exist in the literature showing that differential flatness is a system property defined for a special system output that exhibits no zero dynamics and contains the fundamental system properties rendering possible to control non-minimum phase systems [55], optimal trajectory planning [56], and study of systems containing time delays, [57] and those represented by partial differential equations [58]. Thus, it is expected, and results in this paper verify it, that exploiting differential flatness will result in a plant model with important advantages for controller design.

The remainder of the paper is organized as follows. Linear approximate and differential flatness-based models of the Furuta pendulum are presented in Section II. In Section III the linear state feedback for Furuta pendulum stabilization, the proposed methodology for controller gain selection, and

experimental application on a Furuta pendulum prototype are described. While, the experimental prototype is presented in Section IV. Section V is devoted to describe course where this project is developed, whereas evaluation by students of the project is presented in Section VI. Finally, some concluding remarks are given in Section VII.

## II. FURUTA PENDULUM MODEL

In this section, an approximate linear model for Furuta pendulum is obtained. The goal is to design a linear state feedback controller to stabilize the system at the desired operation point. In order to devise a procedure for suitable controller gain selection, a differential flatness based-model is obtained from the approximate linear model.

The Furuta pendulum –also known as the rotary inverted pendulum– has two degrees of freedom (DOF) and two rotational joints. It is essentially composed by three elements: a motor and two bars called *arm* and *pendulum*. Motor's shaft is fixed at one end of the arm, producing angular arm movements in a horizontal plane. Pendulum is placed at the free end of the arm by means of a joint allowing rotation of pendulum in a vertical plane orthogonal to arm. A representation of the Furuta pendulum is shown in Fig. 1. There, $\theta_0$ is the arm angular position measured with respect to an arbitrary position, $\theta_1$ is the pendulum angular position measured with respect to the upright position, $\tau$ represents torque applied to arm and generated by the motor, $I_0$ stands for motor inertia plus arm inertia (when this turns around an axis orthogonal to one of its ends), $L_0$ is the arm length, $m_1$, $l_1$, and $J_1$ are mass, center of mass location, and inertia (around its center of mass) of pendulum, respectively. Finally, $g$ is acceleration of gravity.

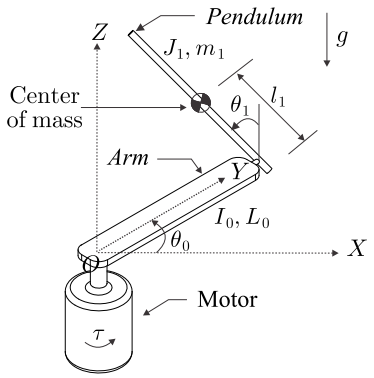


**FIGURE 1.** Furuta pendulum.

The following, complete, nonlinear, Furuta pendulum dynamic model has been obtained in previous works in the literature by invoking Euler-Lagrange equations of motion [35], [36]:

$$M(q)\ddot{q} + C(q,\dot{q})\dot{q} + g(q) = F, \tag{1}$$

where:

$$M(q) = \begin{bmatrix} I_0 + m_1(L_0^2 + l_1^2\sin^2(\theta_1)) & m_1 l_1 L_0\cos(\theta_1) \\ m_1 l_1 L_0\cos(\theta_1) & J_1 + m_1 l_1^2 \end{bmatrix},$$

$$C(q,\dot{q}) = \begin{bmatrix} c_{11} & c_{12} \\ c_{21} & c_{22} \end{bmatrix}, \quad g(q) = \begin{bmatrix} 0 \\ -m_1 l_1 g\sin(\theta_1) \end{bmatrix},$$

$$F = \begin{bmatrix} \tau \\ 0 \end{bmatrix}, \quad q = \begin{bmatrix} \theta_0 \\ \theta_1 \end{bmatrix},$$

$$c_{11} = \frac{1}{2}m_1 l_1^2\dot{\theta}_1\sin(2\theta_1),$$

$$c_{12} = -m_1 l_1 L_0\dot{\theta}_1\sin(\theta_1) + \frac{1}{2}m_1 l_1^2\dot{\theta}_0\sin(2\theta_1),$$

$$c_{21} = -\frac{1}{2}m_1 l_1^2\dot{\theta}_0\sin(2\theta_1), \quad c_{22} = 0.$$

Dynamic model (1) is nonlinear because it includes trigonometric functions of $\theta_1$, as well as different products between arm and pendulum angular velocities, $\dot{\theta}_0$ y $\dot{\theta}_1$, respectively. Since control task to be solved is arm and pendulum position regulation around an operation point, linear control techniques are more suitable because of its simplicity. Thus, an approximate linear model is obtained in the following section.

### A. AN APPROXIMATE LINEAR MODEL

In order to obtain a linear approximate model of (1), which will be only valid around an operation point, the following is needed:

i) The state variable representation of (1), i.e. :

$$\dot{x} = f(x,u),$$

where $x$ and $u$ denote the state vector and the system input, respectively.

ii) To determine the possible system operation points.

The state variable representation of (1) is the following:

$$\begin{bmatrix} \dot{\theta}_0 \\ \ddot{\theta}_0 \\ \dot{\theta}_1 \\ \ddot{\theta}_1 \end{bmatrix} = \begin{bmatrix} \dot{\theta}_0 \\ \frac{(m_1 l_1^2+J_1)(\tau-\rho\dot{\theta}_0\dot{\theta}_1+\sigma\dot{\theta}_1^2)-\gamma\left(\frac{1}{2}\rho\dot{\theta}_0^2+m_1 g l_1\sin\theta_1\right)}{\alpha(m_1 l_1^2+J_1)-\gamma^2} \\ \dot{\theta}_1 \\ \frac{\alpha\left(\frac{1}{2}\rho\dot{\theta}_0^2+m_1 g l_1\sin\theta_1\right)-\gamma(\tau-\rho\dot{\theta}_0\dot{\theta}_1+\sigma\dot{\theta}_1^2)}{\alpha(m_1 l_1^2+J_1)-\gamma^2} \end{bmatrix},$$

where $x = [x_1,x_2,x_3,x_4]^T = [\theta_0,\dot{\theta}_0,\theta_1,\dot{\theta}_1]^T$, $u = \tau$, $f(x,u) = [f_1(x,u),f_2(x,u),f_3(x,u),f_4(x,u)]^T$ is the right-hand vector, and:

$$\alpha = I_0 + m_1 L_0^2 + m_1 l_1^2\sin^2\theta_1, \quad \rho = m_1 l_1^2\sin(2\theta_1),$$
$$\gamma = m_1 L_0 l_1\cos\theta_1, \quad \sigma = m_1 L_0 l_1\sin\theta_1.$$

System operation points, $(\overline{x},\overline{\tau})$, are found by solving:

$$f(\overline{x},\overline{\tau}) = \mathbf{0}. \tag{2}$$

This means that operation points $(\overline{x},\overline{\tau})$ are those values of state $x$ where system can remain without movement, i.e. $\dot{\overline{x}} = \mathbf{0}$, under the effect of a suitable constant system input $\overline{\tau}$, i.e. all components of $\overline{x}$ are constant:

$$\overline{x} = \begin{bmatrix} \overline{\theta}_0 & \dot{\overline{\theta}}_0 & \overline{\theta}_1 & \dot{\overline{\theta}}_1 \end{bmatrix}^T.$$

After solving (2), the following operation points are found:

$$\begin{bmatrix} \overline{\theta}_0 \\ \dot{\overline{\theta}}_0 \\ \overline{\theta}_1 \\ \dot{\overline{\theta}}_1 \end{bmatrix} = \begin{bmatrix} * \\ 0 \\ \pm n\pi \\ 0 \end{bmatrix}, \qquad \overline{\tau} = \overline{u} = 0,$$

where $n = 0, 1, 2, \ldots$, and $*$ represents an arbitrary constant.

Since the pursued control objective is to stabilize pendulum at the upright position, that is, when $\theta_1 = 0$, the following operation point is chosen:

$$\begin{bmatrix} \overline{\theta}_0 & \dot{\overline{\theta}}_0 & \overline{\theta}_1 & \dot{\overline{\theta}}_1 \end{bmatrix}^T = \begin{bmatrix} 0 & 0 & 0 & 0 \end{bmatrix}^T, \quad \overline{\tau} = \overline{u} = 0. \tag{3}$$

Hence, the nonlinear model (1) can be approximated around (3) by the following linear model:

$$\dot{z} = Az + Bv, \tag{4}$$

where:

$$z = \begin{bmatrix} z_1 \\ z_2 \\ z_3 \\ z_4 \end{bmatrix} = \begin{bmatrix} \theta_0 - \overline{\theta}_0 \\ \dot{\theta}_0 - \dot{\overline{\theta}}_0 \\ \theta_1 - \overline{\theta}_1 \\ \dot{\theta}_1 - \dot{\overline{\theta}}_1 \end{bmatrix}, \qquad v = \tau - \overline{\tau} = \tau;$$

and the constant matrices $A$, $B$, are defined as:

$$A = \left[ \begin{array}{cccc} \frac{\partial f_1(x,u)}{\partial x_1} & \frac{\partial f_1(x,u)}{\partial x_2} & \frac{\partial f_1(x,u)}{\partial x_3} & \frac{\partial f_1(x,u)}{\partial x_4} \\ \frac{\partial f_2(x,u)}{\partial x_1} & \frac{\partial f_2(x,u)}{\partial x_2} & \frac{\partial f_2(x,u)}{\partial x_3} & \frac{\partial f_2(x,u)}{\partial x_4} \\ \frac{\partial f_3(x,u)}{\partial x_1} & \frac{\partial f_3(x,u)}{\partial x_2} & \frac{\partial f_3(x,u)}{\partial x_3} & \frac{\partial f_3(x,u)}{\partial x_4} \\ \frac{\partial f_4(x,u)}{\partial x_1} & \frac{\partial f_4(x,u)}{\partial x_2} & \frac{\partial f_4(x,u)}{\partial x_3} & \frac{\partial f_4(x,u)}{\partial x_4} \end{array} \right] \Bigg|_{\substack{x=\overline{x}, \\ u=\overline{u}}}$$

$$= \begin{bmatrix} 0 & 1 & 0 & 0 \\ 0 & 0 & \frac{-gm_1^2 l_1^2 L_0}{I_0(J_1+m_1 l_1^2)+J_1 m_1 L_0^2} & 0 \\ 0 & 0 & 0 & 1 \\ 0 & 0 & \frac{(I_0+m_1 L_0^2) m_1 l_1 g}{I_0(J_1+m_1 l_1^2)+J_1 m_1 L_0^2} & 0 \end{bmatrix},$$

$$B = \left[ \begin{array}{c} \frac{\partial f_1(x,u)}{\partial u} \\ \frac{\partial f_2(x,u)}{\partial u} \\ \frac{\partial f_3(x,u)}{\partial u} \\ \frac{\partial f_4(x,u)}{\partial u} \end{array} \right] \Bigg|_{\substack{x=\overline{x}, \\ u=\overline{u}}} = \begin{bmatrix} 0 \\ \frac{J_1+m_1 l_1^2}{I_0(J_1+m_1 l_1^2)+J_1 m_1 L_0^2} \\ 0 \\ \frac{-m_1 l_1 L_0}{I_0(J_1+m_1 l_1^2)+J_1 m_1 L_0^2} \end{bmatrix}.$$

It is important to say that this approximate linear model is valid only if $z \approx 0$ and $v \approx 0$. This means that the mechanism must remain close to the operation point defined in (3). In this respect, the reader can verify that model in (4) remains without change if $\overline{\theta}_1 = \pm 2\pi$.

### B. A LINEAR DIFFERENTIAL FLATNESS-BASED MODEL

The controllability matrix $C_0$ of the linear system (4) is given as:

$$C_0 = \begin{bmatrix} B & AB & A^2B & A^3B \end{bmatrix}.$$

After carrying out the corresponding computations and reducing terms, the following is found:

$$\det(C_0) = \frac{m_1^4 l_1^4 L_0^2 g^2}{[I_0(J_1 + m_1 l_1^2) + J_1 m_1 L_0^2]^4} \neq 0$$

and, hence, (4) is controllable. According to [59], Ch. 2, this implies that (4) is also differentially flat and its flat output $y$ can be found according to:

$$y = \lambda \begin{bmatrix} 0 & 0 & 0 & 1 \end{bmatrix} C_0^{-1} z, \tag{5}$$

where $\lambda$ is an arbitrary nonzero constant. Having carried out the indicated computations and, by convenience, proposing:

$$\lambda = \frac{g l_1 m_1}{J_1 m_1 L_0^2 + I_0 \left(m_1 l_1^2 + J_1\right)},$$

the flat output is found to be given as:

$$y = z_1 + h z_3, \tag{6}$$

where:

$$h = \frac{J_1 + m_1 l_1^2}{L_0 l_1 m_1}.$$

Differentiating $y$ four times with respect to time and using the linear model (4), the following is found:

$$\dot{y} = z_2 + h z_4, \tag{7}$$

$$\ddot{y} = (a + bh) z_3,$$

$$y^{(3)} = (a + bh) z_4,$$

$$y^{(4)} = b\ddot{y} + d(a + bh)\tau, \tag{8}$$

where:

$$a = \frac{-gm_1^2 l_1^2 L_0}{I_0(J_1 + m_1 l_1^2) + J_1 m_1 L_0^2},$$

$$b = \frac{(I_0 + m_1 L_0^2) m_1 l_1 g}{I_0(J_1 + m_1 l_1^2) + J_1 m_1 L_0^2},$$

$$d = \frac{-m_1 l_1 L_0}{I_0(J_1 + m_1 l_1^2) + J_1 m_1 L_0^2}.$$

Applying Laplace transform to (8), the following transfer function equivalent to (4) is found:

$$\frac{Y(s)}{\tau(s)} = \frac{d(a + bh)}{s^2(s^2 - b)}, \tag{9}$$

where $Y(s)$ and $\tau(s)$ stand for Laplace transforms of flat output and applied torque, respectively. From now on, assume that $d(a + bh) < 0$, which will become true later when replacing numerical values of parameters involved. Transfer function in (9) has four real open-loop poles: two of them located at $s = 0$, one at $s = -\sqrt{b} < 0$, and another at $s = \sqrt{b} > 0$. Recall that $b$ is a positive real number. In the following section, transfer function in (9) is exploited to compute suitable controller gains.

## III. STATE FEEDBACK CONTROL

In Section II was found that linear system (4) is controllable. Then, $\lim_{t\to\infty} z(t) = \mathbf{0}$ can be accomplished using a linear state feedback controller as the following:

$$v = -Kz, \tag{10}$$

where $K = [k_1, k_2, k_3, k_4]$ is the gain vector. According to Section 5, this controller can be written as:

$$\tau = -k_1 z_1 - k_2 z_2 - k_3 z_3 - k_4 z_4. \tag{11}$$

In order to stabilize (4) in closed-loop, $K$ has to be suitably selected. A basic requirement is that the real part of all of the eigenvalues of the closed-loop matrix $A - BK$ be negative. Furthermore, eigenvalues of matrix $A - BK$ must also be assigned such that a desired closed-loop performance be accomplished. Some times it is required to choose a new gain vector $K$ in order to further improve performance. Under ideal conditions this task could be simple, but in practice it results difficult since fast and well damped eigenvalues is not the only thing that matters because of noise and some other problems related to hardware implementation. In that direction, the next section presents a methodology that assists for the selection of the gain vector $K$.

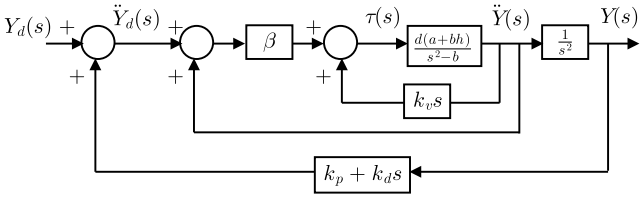


**FIGURE 2.** Block diagram of the closed-loop system.

### A. CONTROL METHODOLOGY FOR SELECTING THE GAIN VECTOR

Assuming that $d(a+bh) < 0$, the multi-loop control scheme shown in Fig. 2 is proposed to control (9). This yields the following closed-loop transfer function:

$$\frac{Y(s)}{Y_d(s)} = \frac{\beta d(a+bh)}{p(s)}, \tag{12}$$

where $Y_d(s) = 0$ is the desired flat output, $p(s)$ is the characteristic polynomial defined as:

$$p(s) = s^4 - d(a+bh)k_v s^3 - (b + \beta d(a+bh))s^2 - \\ -k_d \beta d(a+bh)s - k_p \beta d(a+bh),$$

and $\beta, k_v, k_d, k_p$ are the controller gains. Transfer function of the two internal loops is:

$$\frac{\ddot{Y}(s)}{\ddot{Y}_d(s)} = F(s) = \frac{\beta d(a+bh)}{s^2 - d(a+bh)k_v s - (b + \beta d(a+bh))}. \tag{13}$$

From (12), it is clear that a negative $d(a+bh)$ renders possible that all of the coefficients of $p(s)$ be positive. This is a necessary (but not sufficient) condition for all roots of $p(s)$ to have negative real part.

According to Fig. 2, and by using expressions (7)–(8), the following controller is found:

$$\begin{aligned}\tau &= k_v y^{(3)} + \beta(\ddot{y}_d + \ddot{y}), \\ &= k_v y^{(3)} + \beta(k_p y + k_d \dot{y} + \ddot{y}), \\ &= \beta k_p z_1 + \beta k_d z_2 + (\beta(a+bh) + \beta k_p h) z_3 + \\ &\quad + (k_v(a+bh) + \beta k_d h) z_4. \end{aligned} \tag{14}$$

When comparing (11) and the last expression in (14), the following is concluded:

$$\begin{aligned} k_1 &= -\beta k_p, \\ k_2 &= -\beta k_d, \\ k_3 &= -(\beta(a+bh) + \beta k_p h), \\ k_4 &= -(k_v(a+bh) + \beta k_d h). \end{aligned} \tag{15}$$

Thus, gain vector $K$ can be selected through gains of controller in (14). Procedure to be followed to determine these latter gains is described below.

**TABLE 1.** Numerical parameters of an experimental Furuta pendulum.

| Symbol | Value | Units |
|---|---|---|
| $g$ | 9.81 | m/s$^2$ |
| $l_1$ | $129 \times 10^{-3}$ | m |
| $L_0$ | $155 \times 10^{-3}$ | m |
| $m_1$ | $22.18 \times 10^{-3}$ | Kg |
| $J_1$ | $184.50 \times 10^{-6}$ | Kg m$^2$ |
| $I_0$ | $238.49 \times 10^{-6}$ | Kg m$^2$ |

Using the numerical parameters of a built Furuta pendulum, which are presented in Table 1, the following is found:

$$d(a+bh) = -1.2186 \times 10^5, \quad b = 93.9951.$$

Taking into account these numerical values, $\beta$ and $k_v$ are chosen such that all coefficients of characteristic polynomial in (13) be positive. Moreover, as shall be seen next, it is important that poles of transfer function in (13) have a significant negative real part. Thus, $k_v = 2.3755 \times 10^{-4}$ and $\beta = 0.0041$ have been selected because this assign poles of (13) at $s_{1,2} = -14.4734 \pm 14.0048j$. Note that aside from two poles at $s = 0$, the plant transfer function in (9) has real poles at $s = \pm\sqrt{b} = \pm 9.6951$. Thus, placing poles of (13) at $s_{1,2} = -14.4734 \pm 14.0048j$ ensures stability of this transfer function and, given the proximity of these poles with that at $s = -\sqrt{b} = -9.6951$, a response which is a little faster than that of the open-loop system is also ensured. This is a useful criterion when a desired time response is not specified but an excessively fast response is undesired in order to avoid large noise amplification. Also note that placing poles at $s_{1,2} = -14.4734 \pm 14.0048j$, a damping

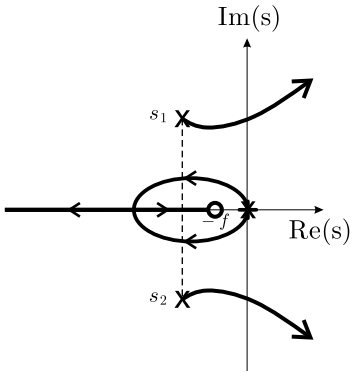


**FIGURE 3.** Root locus diagram for control system in Fig. 2.

coefficient of $\zeta = 0.7186$ is introduced, which is intended to avoid large oscillations. On the other hand, by considering

$$\frac{\pm 180^\circ(2p+1)}{n-m}, \quad p = 0, 1, 2, \ldots$$

where $n = 4$ and $m = 1$, it is found that root locus of block diagram shown in Fig. 2 has three asymptotes: at $\pm 60^\circ$ and $\pm 180^\circ$ angles with respect to the positive real axis. Thus, $f = k_p/k_d = 1$ is proposed in order to shape root locus as indicated in Fig. 3. It is stressed that the open-loop zero at $s = -f$ is not a closed-loop zero as corroborated by (12). Recall that curves in Fig. 3 are parameterized by $k_d$ which grows from 0 to $+\infty$. Hence, $k_d$ is chosen such that the four closed-loop poles be on the left-hand half plane. Note that it is important for this that $s_1$ and $s_2$ have significant negative real parts, as predicted above. It is found that a good value is $k_d = 2.88$. Once this variable is known, $k_p = k_d f = 2.88$ is computed. This gain selection assigns poles of (12) at:

$$-12.1989 \pm 11.8679j, \quad -2.7284, \quad -1.8206.$$

The exact root locus for this case is depicted in Fig. 4, which has been obtained using the following transfer function (see (13) and Fig. 2):

$$\frac{-\beta d(a+bh)}{s^2 - d(a+bh)k_v s - (b+\beta d(a+bh))} \frac{k_p + k_d s}{s^2}, \tag{16}$$

with numerical values in Table 1 and the following controller gains:

$$\begin{aligned} \beta &= 0.0041, \quad k_v = 2.3755 \times 10^{-4}, \\ k_d &= 2.88, \quad k_p = 2.88. \end{aligned} \tag{17}$$

Sign "$-$" in (16) is introduced because positive feedback is used in the external loop of Fig. 2.

Finally, using relations in (15) as well as numerical values in Table 1, the state feedback controller gain vector $K$ is found to be:

$$\begin{aligned} K &= [k_1, k_2, k_3, k_4] \\ &= [-0.0118, -0.0118, -0.2742, -0.0298]. \end{aligned} \tag{18}$$

What it has been presented up to here shows how to use the root locus method to tune the modern controller in (10).

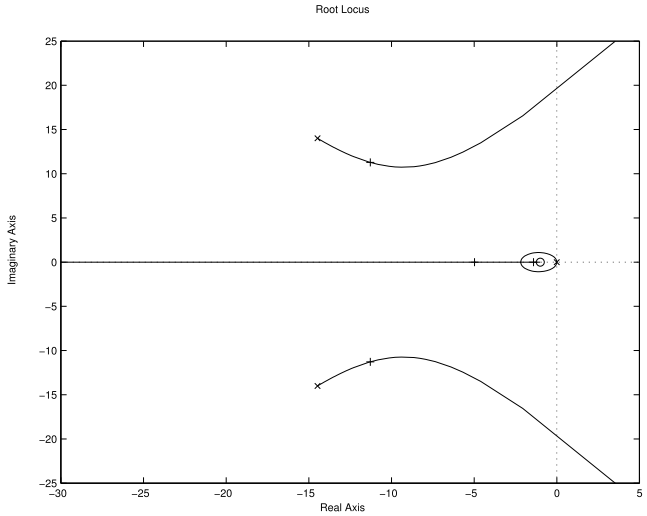


**FIGURE 4.** Root locus diagram for open-loop transfer function in (16).

From this point on, any classical control technique can be used to solve this problem. As an example of application, the remainder of the paper shall focus on using the root locus method to tune controller in (10) in such a manner that performance be improved when a particular control problem appears: oscillation due to limit cycles.

### B. EXPERIMENTAL RESULTS

In order to observe the real behavior of the Furuta pendulum prototype under the influence of the proposed controller and the proposed gains, an experiment was performed. Since (14) only stabilizes the prototype at $z = x - \overline{x} = 0$ when operating close to (3), controller reported in [35], [36], was used to swing-up the pendulum. Such a controller is defined as:

$$\begin{aligned} \tau &= \frac{-\frac{k_\omega}{\det(M(q))}F(q,\dot{q}) - k_\theta\theta_0 - k_\delta\dot{\theta}_0}{k_E E(q,\dot{q}) + \frac{k_\omega}{\det(M(q))}(J_1 + m_1 l_1^2)}, \\ E(q,\dot{q}) &= \frac{1}{2}\dot{q}^T M(q)\dot{q} + m_1 g l_1(\cos\theta_1 - 1), \\ F(q,\dot{q}) &= -(J_1 + m_1 l_1^2)m_1 l_1^2 \dot{\theta}_1\dot{\theta}_0 \sin(2\theta_1) - \\ &\quad - \frac{1}{2}m_1^2 l_1^3 L_0 \dot{\theta}_0^2 \cos\theta_1 \sin(2\theta_1) \\ &\quad - m_1^2 l_1^2 L_0 g \cos\theta_1 \sin\theta_1 + \\ &\quad + (J_1 + m_1 l_1^2)m_1 l_1 L_0 \dot{\theta}_1^2 \sin\theta_1, \end{aligned} \tag{19}$$

where $E(q,\dot{q})$ is the Furuta pendulum total energy (see [35], [36]), $k_\theta > 0$, $k_\delta > 0$, and $k_\omega$, $k_E$, are positive constants that must satisfy:

$$\frac{k_\omega}{k_E} > 2m_1 g l_1 (I_0 + m_1 l_1^2 + m_1 L_0^2).$$

Good results have been obtained with:

$$k_E = 480, \quad k_\omega = 1, \quad k_\delta = 3, \quad k_\theta = 17. \tag{20}$$

Experimental results are shown in Fig. 5, where $i_c$ is electric current through motor and $u_f$ is voltage applied at

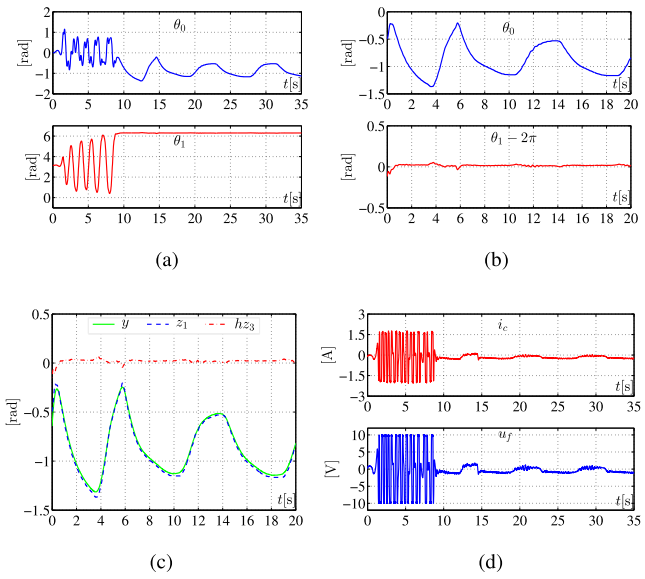


**FIGURE 5.** Experimental results when using (11), (18).

motor terminals. Controller (19), (20), is employed from $t = 0\,[\mathrm{s}]$ to $t = 8.8\,[\mathrm{s}]$, whereas controller (11), (18), is employed for $t > 8.8\,[\mathrm{s}]$. It can be seen that the pendulum reaches position $\theta_1 = 2\pi\,[\mathrm{rad}]$. Since $2\pi\,[\mathrm{rad}]$ represents the same pendulum position when $\theta_1 = 0[\mathrm{rad}]$, this means that the pendulum reaches the desired position and remains there. It is also observed that arm does not stop moving but it describes large peak-to-peak oscillations of about 0.6 [rad] around a constant position of about $-0.8\,[\mathrm{rad}]$. In Figs. 5(b) and 5(c), the time axis was modified in order to consider $t = 0$ at time when the stabilizing controller (11), (18), is switched on, i.e. when $t = 8.8\,[\mathrm{s}]$ in Fig. 5(c). Note that $y$ and $z_1$ remain close to each other while oscillating because $hz_3$ is close to zero (see (6)). These oscillations represent what it is known as a limit cycle, and it is due to a dead zone nonlinearity induced by static friction at the motor shaft. Furthermore, static friction is also responsible for the large constant position value of $-0.8[\mathrm{rad}]$ around which arm oscillations are performed. In order to explain why oscillations are not present in the pendulum position, consider (7), (8), where:

$$y = z_1 + hz_3, \quad \ddot{y} = (a + bh)z_3,$$

and assume that the flat output oscillation is sinusoidal, i.e. $y = Y_0 \sin(\omega t)$ where $Y_0$ is a positive constant representing the oscillation amplitude. It is not difficult to find that, under these conditions:

$$z_1 = Y_0 \left(1 + \frac{h\omega^2}{a + bh}\right) \sin(\omega t),$$
$$z_3 = -Y_0 \frac{\omega^2}{a + bh} \sin(\omega t). \tag{21}$$

This means that $z_3$ is very small if the oscillation frequency is small and $y \approx z_1$. Notice that, in Fig. 5(c), oscillation frequency is, approximately, $\omega = \frac{2\pi}{8.5} = 0.7392[\mathrm{rad/s}]$ which yields $\frac{\omega^2}{a+bh} = 0.0086$. This explains why oscillations are not observed in the pendulum position and why $z_1$ remains close to $y$.

Since limit cycle is the dominant effect under action of controller (11), design efforts will be directed towards limit cycle elimination in the next sections.

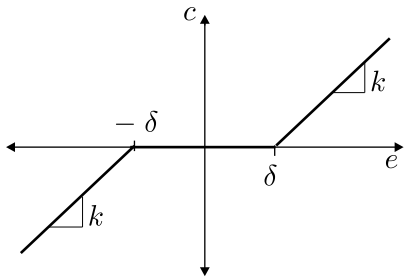


**FIGURE 6.** The dead zone nonlinearity.

### C. DEAD ZONE NONLINEARITY AND LIMIT CYCLES

A dead zone appears at the system input when system does not respond for small values of the input variable, but system begins to respond once input variable exceeds a lower threshold. In mechanical systems this phenomenon is due to static friction. The characteristic function of a dead zone nonlinearity is shown in Fig. 6. The nonlinearity output $c = 0$ when the nonlinearity input $e$ is "small enough", that is, $|e| \leq \delta$ for some $\delta > 0$. For larger values of $e$, the nonlinearity output represents a shifted, amplified version of the nonlinearity input $|c| = k|(e - \delta)|$, $k > 0$.

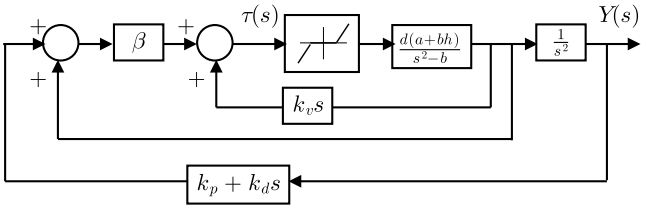


**FIGURE 7.** A closed-loop system including a dead zone nonlinearity.

Fig. 7 presents block diagram in Fig. 2 when a dead zone nonlinearity is considered. Limit cycles are studied using the *describing function method*. For this, it is suggested in [60], Ch. 5, to represent system in the standard form shown in Fig. 8, which is performed by using some block algebra on Fig. 7. The nonlinearity input is $e = \tau(s)$ and the linear time invariant system $G(s)$ is given by:

$$G(s) = \frac{-d(a + bh)(k_v s^3 + \beta s^2 + \beta k_d s + \beta k_p)}{s^2(s^2 - b)}, \tag{22}$$

where $-d(a + bh) > 0$. According to the describing function method, magnitude of (22) must behave as a low-pass filter [60], Ch. 5. This is verified since $G(s)$ has four poles and only three zeros.

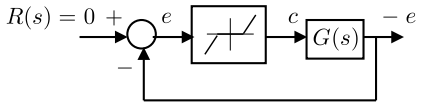


**FIGURE 8.** An equivalent representation for block diagram in Fig. 7.

The describing function is an approximate frequency response description of the nonlinearity which, in the case of a dead zone, is given as [60], Ch. 5:

$$N(A) = \frac{b_1}{A} = \frac{2k}{\pi}\left[\frac{\pi}{2} - \arcsin\left(\frac{\delta}{A}\right) - \frac{\delta}{A}\sqrt{1-\left(\frac{\delta}{A}\right)^2}\right], \tag{23}$$

where $b_1$ is the nonlinearity output amplitude when the nonlinearity input $e$ is assumed to be a sinusoidal function of time with amplitude $A$ and frequency $\omega$. Note that "transfer function" $N(A)$ is real, positive, frequency independent but dependent on input amplitude $A$. Moreover, the maximal value is $N(A) = k > 0$ which is reached as $A \to \infty$. The minimal value tends to zero and it is approached as $A \to \delta$.

According to the describing function method a limit cycle exists if:

$$G(j\omega) = -\frac{1}{N(A)}. \tag{24}$$

Since $N(A)$ is real and positive, $-1/N(A)$ is real and negative. In consequence, a limit cycle exists if polar plot of $G(j\omega)$ intersects the negative real axis in the open interval $(-\infty, -1/k)$. The oscillation frequency and amplitude of the oscillation are found as the values of $\omega$, in $G(j\omega)$, and $A$, in $-1/N(A)$, at point where their plots intersect.

### D. CONTROLLER DESIGN TO AVOID LIMIT CYCLES

In experiments shown in Fig. 5 is observed that oscillation that appears is slow and it has a wide amplitude. This suggests that oscillation might be reduced or eliminated if stiffness of the closed-loop system is increased. Since stiffness is related to faster responses, this also suggests that the oscillation frequency should be increased. On the other hand, since system does not respond if $|e| \leq \delta$ and the dead zone threshold $\delta > 0$ is uncertain, because of the uncertain character of static friction, it is wondered whether oscillation might disappear if the oscillation amplitude is rendered small enough. Thus, in the following a procedure intended to increase frequency and to decrease amplitude of oscillations due to limit cycle is formulated.

According to previous section, in order to obtain a limit cycle with smaller amplitude, polar plot of the equivalent open-loop transfer function $G(s)$ must intersect the negative real axis at a point $\sigma$ located farther to the left. On the other hand, in order to increase the oscillation frequency, phase of $G(j\omega)$ must reach $-180°$ at a larger frequency $\omega = \omega_\sigma$.

Point $\sigma$ can be placed farther at the left of the negative real axis by increasing magnitude of $G(s)$. According to (22) this requires to increase controller gains $k_v$ and $\beta$. On the other hand, according to Fig. 11, $G(j\omega)$ reaches a $-180°$ phase at larger frequencies if phase lead introduced by controller is forced to appear at larger frequencies. Since cubic and quadratic terms in $G(s)$ introduce larger phase leads at larger frequencies, this phase lead can be forced to appear at larger frequencies by rendering coefficients of the first order term and the constant term larger than coefficients of cubic and quadratic terms, i.e. by increasing $k_d$ and $k_p$.

**TABLE 2.** Numerical values used for $G(s)$ defined in (22).

| | Controller gains |
|---|---|
| a) | $k_v = 2.3755 \times 10^{-4}$, $\beta = 0.0041$, $k_d = 2.88$, $k_p = 2.88$ |
| b) | $k_v = 1.2 \times 2.3755 \times 10^{-4}$, $\beta = 1.4 \times 0.0041$, $k_d = 4.59$, $k_p = 4.59$ |
| c) | $k_v = 1.4 \times 2.3755 \times 10^{-4}$, $\beta = 1.8 \times 0.0041$, $k_d = 5.62$, $k_p = 5.62$ |

Based on the aforementioned ideas, three sets of controller gains were computed which are shown in Table 2. In this table, the set of controller gains a) corresponds to gains in (17). The remaining controller gains have been obtained proceeding as follows. In order to increase system stiffness, the closed-loop poles are moved farther to the left of the imaginary axis. This suggests to move the open-loop zero at $s = -f$ to the left (see Fig. 3). However, this may create two root locus branches starting at the origin but belonging to the right half plane. This is because zero at $s = -f$ might attract the open-loop complex conjugate poles at $s_1, s_2$, if it moves to the left. Hence, instability or bad damped closed-loop poles might result if $f > 0$ is increased. Thus, it is proposed to maintain $f = 1$ and only to move to the left the three fastest closed-loop poles.

First, larger values for $k_v$ and $\beta$ are proposed in order to render larger both the real and the imaginary parts of the open-loop poles $s_1$ and $s_2$ in Fig. 3 (also see $s_{1,2}$ in Table 3). This renders faster and well damped the pendulum response[1] and allows selecting larger values for both $k_d$ and $k_p$. This is because, although the root locus branches starting at $s_1$ and $s_2$ move towards the right half plane as $k_d$ increases, it is possible to select larger values for $k_d$ before these branches be too close to the right half plane if $s_1$ and $s_2$ move to the left. Notice that $k_p$ is larger if $k_d$ is larger because $k_p = k_d f$, $f = 1$. In order to clarify these ideas, Figs. 9 and 10 present root locus diagrams obtained when using transfer function in (16) and controller gains in Table 2 (also see Fig. 4).

[1] Notice, in Fig. 2, that $k_v$ and $\beta$ are the feedback gains of signals $\ddot{y}$ and $y^{(3)}$ which, according to (7)–(8), represent feedback of the pendulum position and velocity, $z_3 = \theta_1 - \overline{\theta}_1$ and $z_4 = \dot{\theta}_1$.

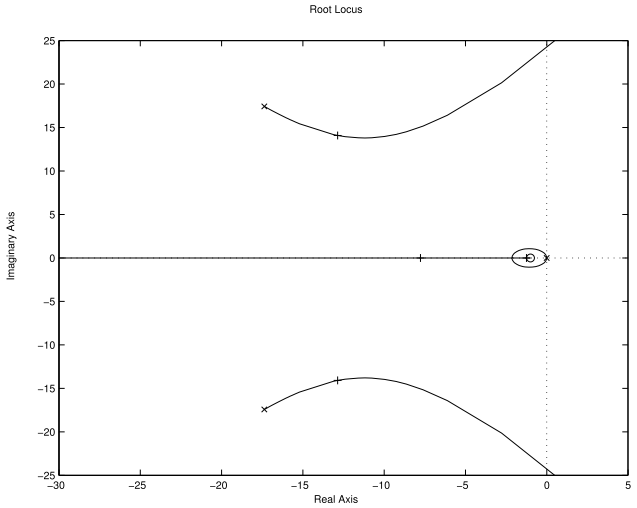


**FIGURE 9.** Root locus diagram for open-loop transfer function in (16) and controller gains in Table 2b).

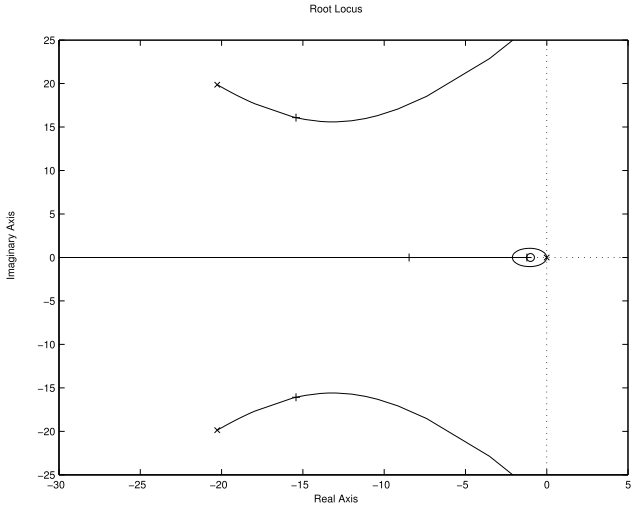


**FIGURE 10.** Root locus diagram for open-loop transfer function in (16) and controller gains in Table 2c).

It is stressed that all poles of (13) shown in Table 3 introduce damping coefficients between 0.7 and 0.8 and, hence, only small oscillations are expected. Also note, in Figs. 9 and 10, that placing poles of (13) farther to the left results in poles of (12) located farther to the left, as expected.

Using controller gains in Table 2 and (15), the controller gains in Table 4 were computed. Notice, in Table 3, that the three fastest closed-loop poles move to the left when going from a) to c) in Table 3 or, equivalently, in Table 4.

In Fig. 11, Bode plots of transfer function in (22) are presented when using numerical values in Tables 1 and 2. As it can be seen in Fig. 11 all of phase plots intersect the $-180°$ phase line. This indicates that a limit cycle exists in all of the cases presented in Table 2. Furthermore, this happens when the $G(s)$ magnitude is larger than 0[dB]. It is recalled that the open interval $(-\infty, -1/k)$ corresponds to

**TABLE 3.** Assigned open-loop and closed-loop poles.

| Controller gains | Poles of (13) | Poles of (12) |
|---|---|---|
| a) | $s_{1,2} = -14.4734 \pm 14.0048j$ | $-12.1989 \pm 11.8679j$, $-2.7284$, $-1.8206$ |
| b) | $s_{1,2} = -17.3681 \pm 17.4300j$ | $-13.535 \pm 14.37j$, $-6.3736$, $-1.2926$ |
| c) | $s_{1,2} = -20.2628 \pm 19.8676j$ | $-15.5358 \pm 16.1280j$, $-8.2292$, $-1.2247$ |

**TABLE 4.** State feedback controller gains.

| | Controller gains |
|---|---|
| a) | $k_1 = -0.0118$<br>$k_2 = -0.0118$<br>$k_3 = -0.2742$<br>$k_4 = -0.0298$ |
| b) | $k_1 = -0.0263$<br>$k_2 = -0.0263$<br>$k_3 = -0.3962$<br>$k_4 = -0.0509$ |
| c) | $k_1 = -0.0415$<br>$k_2 = -0.0415$<br>$k_3 = -0.5189$<br>$k_4 = -0.0728$ |

the open interval $(0, \infty)$[dB] (because $k = 1$ is assumed) when phase is $-180°$. Also, it is stressed that the $-180°$ phase line is intersected at a larger frequency as the controller gains from a) to c) in Table 2 are considered. Moreover, according to Fig. 12 the negative real axis is intersected by the polar plot of $G(j\omega)$ at some point, which moves to the left when going from a) to c) in Table 2. Thus, it is concluded that the oscillations amplitude decreases and oscillations frequency increases when going from a) to c) in Table 2 or, equivalently, in table 4.

Evolution in simulation of flat output $y(t)$ in Fig. 7 is presented in Fig. 13, when the numerical values in Table 2 are used as well as $k = 1$ and the arbitrary value $\delta = 0.0115$. All of the initial conditions were set to zero excepting $y(0) = 1$. These results verify all of the above predictions. It is important to remark that the above theoretical discussion on limit cycles was intended to explain amplitude and frequency of oscillation at input of nonlinearity $e = \tau(s)$. However, in Fig. 13 the oscillation of the different variable $y$ which relates to $e = \tau(s)$ through $e = -(k_v s^3 + \beta s^2 + \beta k_d s + \beta k_p)Y(s)$ is presented. Hence, it is clear that, due to the linear relation between $e$ and $y(t)$, these results are also valid for $y(t)$.

### E. MORE EXPERIMENTAL RESULTS

Figs. 14 and 15 show experimental results obtained when using controller gains b) and c), respectively, in Table 4. In Figs. 14(b) and 14(c), $t = 0$ was set at the point of time

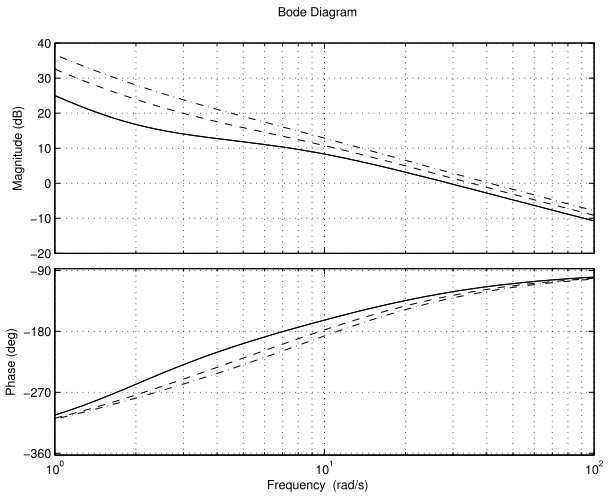


**FIGURE 11.** Bode plots of $G(s)$ in (22) when using the numerical values in Table 2. Continuous a). Dashed b). Dash-dot c).

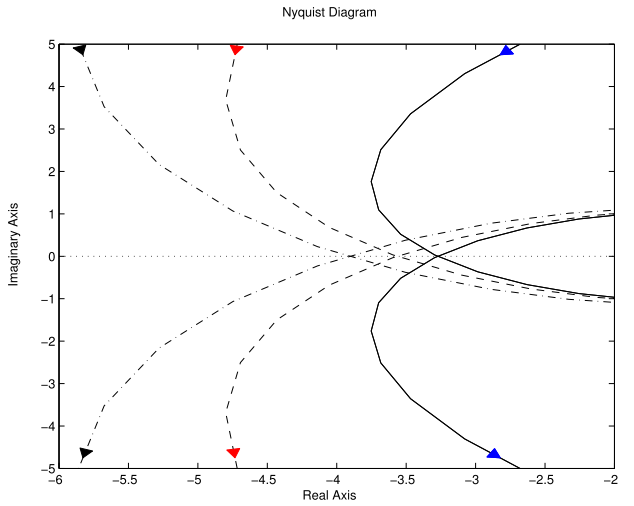


**FIGURE 12.** Polar plot of $G(s)$ in (22) when using the numerical values in Table 2. Continuous a). Dashed b). Dash-dot c).

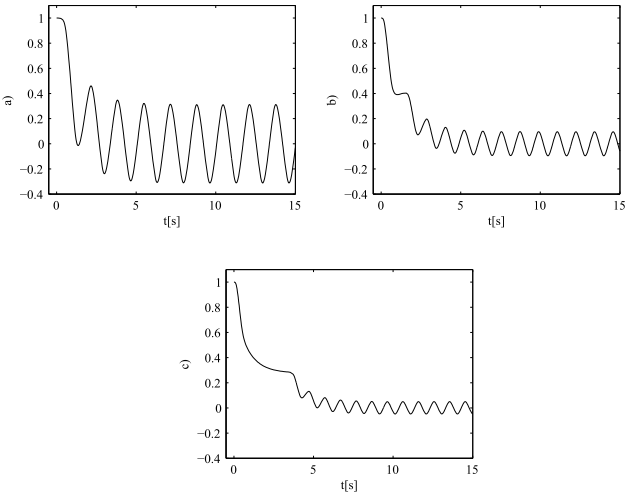


**FIGURE 13.** Simulation response of flat output $y$ in Fig. 7 when using numerical values in Table 2.

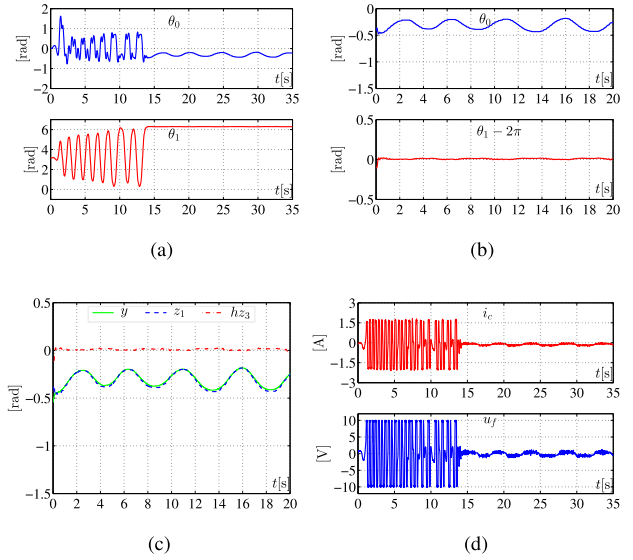


**FIGURE 14.** Experimental results when using controller gains in Table 4b).

$t = 13.8$[s] in Fig. 14(a) (when controller (11) is switched on). Also, in Figs. 15(b) and 15(c), $t = 0$ was set at the point of time $t = 12.9$[s] in Fig. 15(a) (when controller (11) is switched on).

These results show that the pendulum position is successfully stabilized at $\theta_1 = 2\pi$. On the one hand, when gains b) of Table 4 are used, the following is observed. Although the arm position still oscillates, the amplitude is smaller and frequency $\omega = 2\pi/5 = 1.2566$[rad/s] is larger than values in Fig. 5. Also, oscillations are performed around a constant arm position of about $-0.35$[rad], which is smaller than in the case of controller gains a). The above values yield $\frac{\omega^2}{a+bh} = 0.0250$ which explains, again, why oscillations do not appear in the pendulum position. On the other hand, when gains c) are used, in Fig. 15, limit cycle disappears. As can be seen in Figs. 15(a), 15(b), 15(c), the oscillation amplitude in both the flat output $y$ and the arm position $\theta_0$ are even smaller whereas the oscillation frequency has increased to about $\omega = 2\pi/2.3 = 2.7318$[rad/s]. Furthermore, both of these variables reach constant values, i.e. oscillation disappears, for $t \geq 7$[s] in Figs. 15(b) and 15(c). The pendulum position reaches its desired constant value. Also a constant steady state error in the arm position about 0.2[rad] is observed, i.e. even smaller than the mean error of $-0.35$[rad] for controller gains b) in Table 4. It is important to remark that the small threshold $\delta$ in a dead zone nonlinearity is uncertain and changes during normal operation. This is because the static friction also has these properties. Since any movement is not produced when the generated torque is smaller than $\delta$ (or the applied voltage is small enough), it may wonder whether limit cycles might be avoided by forcing them to appear only at a very small amplitudes. Hence, this might explain why limit cycle has disappeared.

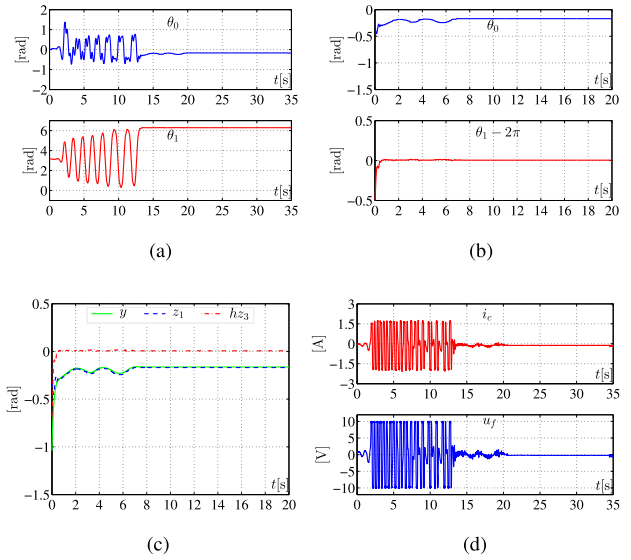


**FIGURE 15.** Experimental results when using controller gains in Table 4c).

**FIGURE 16.** Furuta pendulum built at the Control Systems Laboratory of Universidad Autónoma de Querétaro.

Even though the limit cycle has disappeared when using the gain set c), it is stressed that the limit cycle avoidance is not achieved all of the times that an experiment is performed with such a controller gains. Some times very small and very slow oscillations are observed on both $z_1$ and $y$ whereas $z_3$ remains at zero without oscillations. Thus, limit cycle avoidance appears as a random event perhaps because the small threshold $\delta$ is uncertain and changes during normal operation.

## IV. EXPERIMENTAL PROTOTYPE

All of the above experiments were performed using a Furuta pendulum prototype built at the Control Systems Laboratory of Universidad Autónoma de Querétaro, whose numerical parameters are shown in Table 1. Fig. 16 presents a picture of this Furuta pendulum and the complete electric diagram is presented in Fig. 17. Control algorithm is implemented in a Builder 6 C++ program which is executed by a personal computer. The personal computer receives the mechanism output data from a PIC16F877A microcontroller and sends back to the microcontroller the mechanism input data. Then, microcontroller sends to motor the corresponding voltage signal. Both, personal computer and microcontroller work at a 0.01[s] sampling period. It is recognized that this is a large sampling period. However, it must be stressed that, according to our experience with different Furuta pendulum prototypes, a large sampling period is recommendable to accomplish limit cycle elimination. Moreover, it was also found in simulations that, in the case a limit cycle is eliminated, addition of noise to position measurements results again in oscillations due to a limit cycle. Interestingly enough is that it was also observed in experiments that noise is more appreciable when using a small sampling period.

An L298 integrated circuit containing two full-bridge drivers, which are parallel connected, is used as power amplifier. Three AND logic gates manage the enable bits for the L298 full-bridge. The power signal is applied on a permanent magnet brushed DC motor, model Tohoko Ricoh 7K00011, which is employed as the mechanism actuator. This motor is provided with a 400 pulses/revolution encoder, which is used to measure the arm position. The pendulum position is measured by a 1000 pulses/revolution encoder, model S1-1000-250-I-B-D from USDigital (bottom encoder in Fig. 17). Velocity of both arm and pendulum is estimated by numerical differentiation, i.e. $\omega_v = \frac{\Delta\theta}{\Delta t}$, where $\theta$ stands for position of either arm or pendulum, $\omega_v$ is velocity of either arm or pendulum, $\Delta\theta = \theta_k - \theta_{k-1}$, with $k$ standing for discrete time, and $\Delta t = 0.01$[s] is sampling period. Communication between personal computer and microcontroller is rendered possible by a MAX232. Finally, the complete control system is put to work through SWITCH_1.

The mechanism is provided with an electric current loop driven by a porportional-integal (PI) controller driven by the difference $i_d - i_c$, where $i_c$ is electric current through the motor armature and $i_d$ is the desired current. The PI controller is implemented in the personal computer program with 0.8 as the proportional gain and 130 as the integral gain. The desired current is computed as $i_d = \tau/k_m$, where $\tau$ is obtained from either (19) or (11) and $k_m = 0.0368$[Nm/A]. This ensures that $i_c \approx i_d$ for all time and, hence, torque generated by motor approximately equals the desired torque given by either (19) or (11). Electric current through the motor armature $i_c$ is converted to a voltage signal by a 1[Ω]/5[W] power resistance, which is series connected to motor armature terminals. This voltage is measured by the differential voltage amplifier located at the left upper corner in Fig. 17. After that, this signal is suitably amplified and a summing amplifier is used to center the zero current value at a +2.5[V] level. Then, the measured current is low-pass filtered and sent to a 10 bit analogue-to-digital converter in the microcontroller, whose input analogue range is $[0, +5]$[V]. This allows to measure electric current in the range $[-2.5, +2.5]$[A]. Recall that the 1[Ω] power resistance converts electric current into a

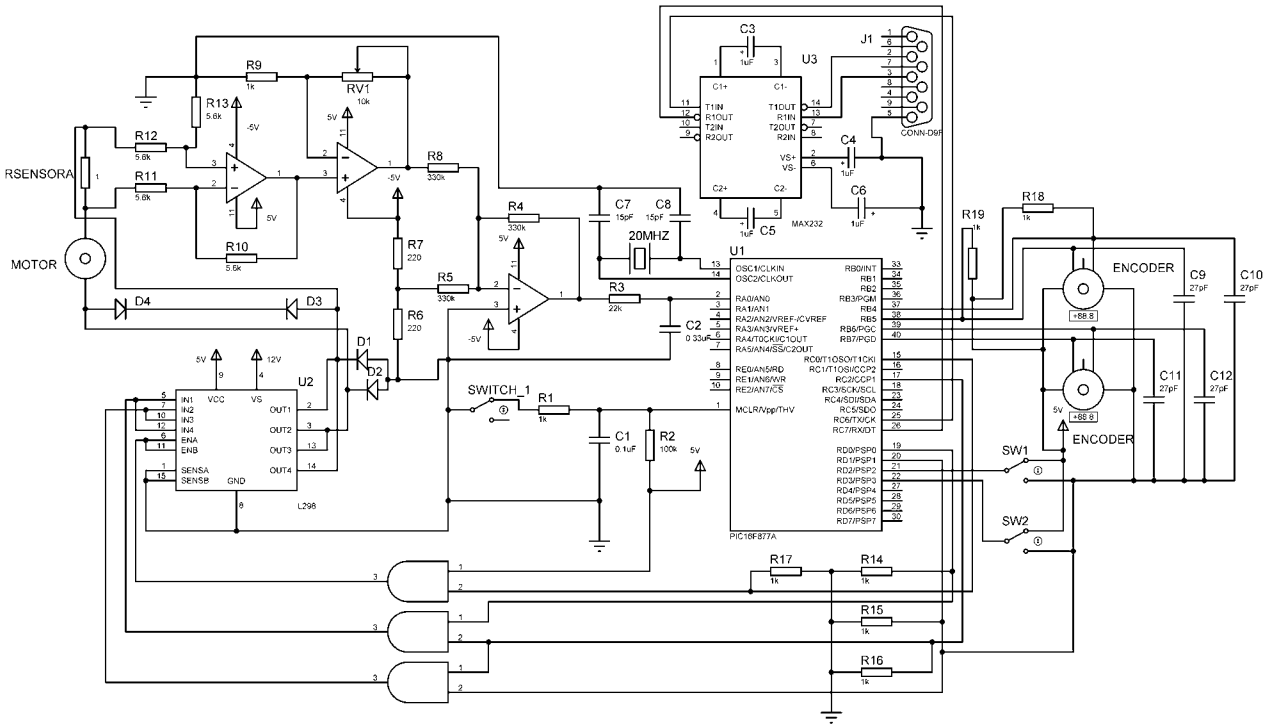


**FIGURE 17.** Electric diagram of Furuta pendulum used in experiments.

voltage signal whose numerical value equals electric current in Amperes.

Condition to switch on the stabilizing controller (11) is set as $3(\theta_1 - \text{teta1d})^2 + \dot{\theta}_1^2 < 0.05$, where teta1d equals either 0[rad] or $2\pi$[rad], i.e. the pendulum upward position. If this is not the case then controller (19) is kept working. In all of the experiments reported in this paper the initial conditions $[\theta_0, \dot{\theta}_0, \theta_1, \dot{\theta}_1] = [0, 0, \pi, 0]$ were fixed at the time when controller (19) starts to work. According to theory on controller (19), reported in [35], [36], an initial "kick" signal is required to start the swing-up motion. It was observed in the experiments that this "kick" signal automatically appears at the moment when turning on the power supply. As it can be observed from Figs. 14 and 15, controller (19) accomplishes the swing-up task in approximately the same time. However a difference of about 5[s] exists between time required in these figures and time required in Fig. 5. This difference in time might be attributed to *i*) the large sampling period used in experiments (because of limit cycle elimination reasons, as explained above), i.e. 0.01[s], *ii*) saturation of applied voltage, or *iii*) a different "kick" signal. However, it is also important to remember that (nonlinear) friction has not been taken into account in [35], [36] when designing controller (19). Consider, for instance, Fig. 14(a) where it is clear that oscillation of $\theta_1$ has not an ever growing amplitude. Moreover, it is observed in figs. 14(a) and 15(a) that controller (11) could be switched on at about $t = 10$[s], but this was not the case. Such a behavior can be attributed to friction. Any way, it must be stressed that study of performance of controller (19) is not the aim of the present work and it is employed here just to provide suitable initial conditions to test controller (11). Although these initial conditions are not the same in all experiments, they are not artificial in the sense that they are not specially selected just to show that an experiment works well. On the contrary, these initial conditions are realistic in the sense that they result from a previous swing-up task and the stabilizing controller works well when starting from such non a priori known initial conditions.

## V. COURSE DESCRIPTION

The Engineering Faculty of Universidad Autónoma de Querétaro at Querétaro, México, offers the Automation Engineering major. As a part of the curricula, in the fifth and sixth semesters, the enrolled students attend the subjects Control I and Control II, respectively. Control I is a course composed by three hours a week lectures on theoretical aspects of the time response approach of classical control systems: first and second order systems, block algebra, Routh stability criterion, the steady state error, and analysis and design using root locus. Additionally, a one hour a week laboratory session is included where students gain experience on system modelling, system response simulation, control systems analysis and design, and experimental controller implementation using both analogue (operational amplifiers) and digital (personal computer and microcontrollers) electronics. As a final project, students model and experimentally identify a ball and beam system, design a controller using root locus and, finally, experimentally test controller that they have designed

**TABLE 5. Student evaluation.**

| Question | Average score | 5 | 4 | 3 | 2 | 1 |
|---|---|---|---|---|---|---|
| 1.- Generalities of the Furuta pendulum system are well presented | 4.71 | 71.43% | 28.57% | 0 | 0 | 0 |
| 2.- Information about the dynamic model and its linear approximation is enough to understand them | 4.57 | 57.14% | 42.86% | 0 | 0 | 0 |
| 3.- Information related to differential flatness is clearly explained | 4.43 | 42.86% | 57.14% | 0 | 0 | 0 |
| 4.- Simulation of the system dynamic model improves knowledge | 4.43 | 57.14% | 28.57% | 14.29% | 0 | 0 |
| 5.- Skills are improved by practicing with a real prototype | 4.71 | 71.43% | 28.57% | 0 | 0 | 0 |
| 6.- Practicing with a real prototype helps to better understand theory discussed in classroom | 4.86 | 85.71% | 14.29% | 0 | 0 | 0 |
| 7.- The proposed methodology renders easier selection of controller gains | 4 | 28.57% | 42.86% | 28.57% | 0 | 0 |
| 8.- The proposed methodology is useful to better understand application of root locus for controller design | 4.14 | 42.86% | 28.57% | 28.57% | 0 | 0 |
| 9.- The proposed problem is useful to better understand frequency response tools | 4.29 | 28.57% | 71.43% | 0 | 0 | 0 |
| 10.- The acquired knowledge on linear state feedback control is enough for application to other linear systems | 3.43 | 0 | 57.14% | 28.57% | 14.29% | 0 |
| 11.- The acquired knowledge on dead zone and limit cycles is useful for control of mechanisms | 3.29 | 28.57% | 14.29% | 14.29% | 42.86% | 0 |

using a computer to implement the control algorithm and a microcontroller-based acquisition board built in the laboratory sessions.

Control II is divided in two parts: the classical frequency response approach of control systems and the modern control state variable approach for linear systems. This course is composed by four hours a week lectures on theoretical aspects of these subjects and one hour a week is devoted to laboratory. In laboratory, students perform experiments with passive filters as a manner to understand what frequency response means, they experimentally identify a brushed DC motor using its frequency response and, based on these results, they design a proportional-integral velocity controller and a proportional-integral-derivative position controller. They are also introduced to limit cycle phenomenon by studying its effects when controlling position of an inertia actuated by a brushed DC motor through a rotational spring. As a project for the frequency response approach, they design and experimentally test a controller for the ball and beam system. Second part of semester in laboratory is focused to control the Furuta pendulum as exposed in the present paper. With this aim, theoretical lectures on the state variable approach are focused on state variables definition and model representation, stability, controllability and observability, linear static state feedback control, linear feedback using observers, and differential flatness.

Although differential flatness might seem too elaborated for a first course on the state variable approach, exposition of the subject is simplified by focusing on the strictly necessary tools for application to Furuta pendulum. For instance, a linear differentially flat system is defined just as a controllable linear system. Then, result in [59], Ch. 2 is presented, i.e. expression in (5) as the manner to find the flat output. Using these ideas and all of the previous subjects studied in both Control I and Control II courses, students are capable to understand all of the concepts presented in this paper.

Since the main subject of both Control I and Control II courses are linear control systems, the linear approximate model of the Furuta pendulum is not deduced but it is just described in classroom, highlighting main attributes such as local validity, system order, state variables and input variables, controllability, differential flatness property, and proportional-integral control of electric current. The students are motivated to see model deduction in [35], [36]. Students are organized in groups and guided to simulate the dynamic model of the Furuta pendulum in the Matlab-Simulink environment. For this, they are provided with the complete nonlinear model of the Furuta pendulum which is used by them as a black box with an input and state variables as output. This is with the intention to understand the behavior of the system. Students are asked to select controller gains for controller in (11) with the only direction that real part of all eigenvalues of matrix $A - BK$ must be negative. The proposed controllers must be simulated in closed-loop with the nonlinear model of the Furuta pendulum. This is intended for students to realize that this is not a simple task and some methodology rendering it easier would be useful. Then, students are asked to obtain transfer function in (9). Subsequently, they are encouraged to apply the methodology herein presented for tuning a linear controller that regulates the Furuta pendulum in the upright position. When the controller design and its corresponding tuning are approved by the subject professor, the students proceed to simulate the system in closed-loop. Once their professor has verified that a good performance is obtained in simulation, students are allowed to test their design in the Furuta Pendulum prototype associated with Figs. 16 and 17.

To do this, students only have to replace their controller gains in the Builder 6 C++ program that is provided by professor. This avoids equipment damage due to uncarelessness of students. Finally, the students have to carry out a report, where they explain with their own words what they have understood about the Furuta pendulum system, control methodology, gain selection using root locus, and behavior of the closed-loop system.

## VI. EVALUATION

After experimentally controlling the Furuta pendulum, the fourteen students enrolled in the course Control II were asked to answer a questionnaire to evaluate the course. The obtained results are presented in Table 5. There, a scale from 1 to 5 was used to indicate dreadful, bad, regular, good, and excellent, respectively. Most students have found that tuning a linear state feedback for the Furuta pendulum is difficult when the only direction is to render negative real part of all eigenvalues of a matrix. They have explained that this is specially true because they have performed simulations using the complete nonlinear model of the Furuta pendulum. In such a scenario actuator saturation and large state variables values may appear when using large controller gains which avoids success of the control task. On the other hand, the proposed methodology renders easier controller gains selection. Besides, they have found that solving this control problem clarifies use of classical control tools such as root locus and frequency response. The above is sustained by the obtained average score which is found between 3.29 and 4.86 points, that is, the course was evaluated as regular to excellent. Therefore, it is concluded that the proposed activities related to the design of a linear state regulator for the Furuta pendulum by using differential flatness and root locus are positive and effective to enhance the understanding and grasping of knowledge in students.

## VII. CONCLUSION

This paper has presented a control methodology to tune a linear state feedback regulator for the Furuta pendulum. This has been accomplished exploiting the Furuta pendulum differential flatness property and using classical control design tools such as the root locus method. The proposed approach has been used to prove existence of a limit cycle induced by static friction at shaft of motor used as actuator. Then, our proposal has been focused to improve closed-loop system performance by reducing or even eliminating effects of limit cycles. Experimental results show that the proposed methodology successfully improves closed-loop performance by reducing and, eventually, eliminating effects of limit cycles.

Students have found that the proposed controller tuning methodology renders easier to learn control design techniques. Reason for this is that our proposal relies on clear classical control ideas to give insight on how to select controller gains. Furthermore, students believe that use of classical control design tools allow them to understand and validate by practice classical control concepts.

## REFERENCES

[1] J. F. Haffner, L. F. Alves Pereira, and D. Ferreira Coutinho, "Computer-assisted evaluation of undergraduate courses in frequency-domain techniques for system control," *IEEE Trans. Educ.*, vol. 49, no. 2, pp. 224–235, May 2006.
[2] A. Leva and F. Donida, "Multifunctional remote laboratory for education in automatic control: The CrAutoLab experience," *IEEE Trans. Ind. Electron.*, vol. 55, no. 6, pp. 2376–2385, Jun. 2008.
[3] J. Sánchez, S. Dormido-Canto, G. Farias, F. Godoy, and S. Dormido, "Understanding automatic control concepts by playing game," *Int. J. Eng. Edu.*, vol. 27, no. 3, pp. 528–534, 2011.
[4] J. L. Guzman, S. Dormido, and M. Berenguel, "Interactivity in education: an experience in the automatic control field," *Comput. Appl. Eng. Edu.*, vol. 21, no. 2, pp. 360–371, 2013.
[5] J. de Jesus Rangel-Magdaleno, J. R. Rivera-Guillen, R. de Jesus Romero-Troncoso, and R. A. Osornio-Rios, "FPGA-MATLAB-based open core for three-time controllers in automatic control applications," *Comput. Appl. Eng. Edu.*, vol. 21, no. S1, pp. E132–E140, 2013.
[6] W. Hu, G.-P. Liu, and H. Zhou, "Web-based 3-D control laboratory for remote real-time experimentation," *IEEE Trans. Ind. Electron.*, vol. 60, no. 10, pp. 4673–4682, Oct. 2013.
[7] J. Sáenz, J. Chacón, L. De Le Torre, A. Visioli, and S. Dormido, "Open and low-cost virtual and remote labs on control engineering," *IEEE Access*, vol. 3, pp. 805–814, 2015.
[8] M. S. Ayas and I. H. Altas, "A virtual laboratory for system simulation and control with undergraduate curriculum," *Comput. Appl. Eng. Edu.*, vol. 24, no. 1, pp. 122–130, 2016.
[9] E. Cuevas, D. Zaldivar, and M. Pérez-Cisneros, "Low-cost commercial Lego platform for mobile robotics," *Int. J. Elect. Eng. Edu.*, vol. 47, no. 2, pp. 132–150, 2010.
[10] Khairurrijal, M. Abdullah, and M. Budiman, "Home-made PIC 16F877 microcontroller-based temperature control system for learning automatic control," *Comput. Appl. Eng. Edu.*, vol. 19, no. 1, pp. 10–17, 2011.
[11] B. Dandil, "An integrated electrical drive control laboratory: Speed control of induction motors," *Comput. Appl. Eng. Edu.*, vol. 20, no. 3, pp. 410–418, 2012.
[12] J. J. Fuertes, M. Domínguez, M. A. Prada, S. Alonso, and A. Morán, "A virtual laboratory of D.C. motors for learning control theory," *Int. J. Elect. Eng. Edu.*, vol. 50, no. 2, pp. 172–187, 2013.
[13] M. Casini, A. Garulli, A. Giannitrapani, and A. Vicino, "A remote lab for experiments with a team of mobile robots," *Sensors*, vol. 14, no. 9, pp. 16486–16507, 2014.
[14] M. Domínguez, J. J. Fuertes, M. A. Prada, S. Alonso, and A. Morán, "Remote laboratory of a quadruple tank process for learning in control engineering using different industrial controllers," *Comput. Appl. Eng. Edu.*, vol. 22, no. 3, pp. 375–386, Sep. 2014.
[15] J. A. Frank and V. Kapila, "Development of mobile interfaces to interact with automatic control experiments," *IEEE Control Syst. Mag.*, vol. 34, no. 5, pp. 78–98, Oct. 2014.
[16] M. A. Prada, J. J. Fuertes, S. Alonso, S. García, and M. Domínguez, "Challenges and solutions in remote laboratories. Application to a remote laboratory of an electro-pneumatic classification cell," *Comput. Edu.*, vol. 85, pp. 180–190, Jul. 2015.
[17] J. M. Giron-Sierra, "A simple device and a project for the nonlinear control systems laboratory," *IEEE Trans. Educ.*, vol. 44, no. 2, pp. 144–150, May 2001.
[18] J. Sanchez, S. Dormido, R. Pastor, and F. Morilla, "A Java/MATLAB-based environment for remote control system laboratories: Illustrated with an inverted pendulum," *IEEE Trans. Educ.*, vol. 47, no. 3, pp. 321–329, Aug. 2004.
[19] A. A. Rodriguez, R. P. Metzger, O. Cifdaloz, and T. Dhirasakdanon, "Description of a modeling, simulation, animation, and real-time control (MoSART) environment for a class of electromechanical systems," *IEEE Trans. Educ.*, vol. 48, no. 3, pp. 359–374, Aug. 2005.
[20] J. Petrić and Z. Šitum, "Pneumatic balancing mechanisms in control education," *Int. J. Eng. Edu.*, vol. 22, no. 6, pp. 1297–1303, 2006.
[21] G.-H. Lee, J.-S. Noh, and S. Jung, "Implementation and experiment of neural network controllers for intelligent control system education," *Int. J. Fuzzy Logic Intell. Syst.*, vol. 7, no. 5, pp. 267–273, 2007.
[22] G.-H. Lee and S. Jung, "Neuro-fuzzy control of inverted pendulum system for intelligent control education," *Int. J. Fuzzy Logic Intell. Syst.*, vol. 9, no. 4, pp. 309–314, 2009.

[23] S.-C. Lin and C.-C Tsai, "Development of a self-balancing human transportation vehicle for the teaching of feedback control," *IEEE Trans. Educ.*, vol. 52, no. 1, pp. 157–168, Feb. 2009.

[24] M. Stefanovic, M. Matijevic, V. Cvijetkovic, and V. Simic, "Web-based laboratory for engineering education," *Comput. Appl. Eng. Edu.*, vol. 18, no. 3, pp. 526–536, 2010.

[25] M. J. Mahmoodabadi, A. Bagheri, S. A. Mostaghim, and M. Bisheban, "Simulation of stability using Java application for Pareto design of controllers based on a new multi-objective particle swarm optimization," *Math. Comput. Model.*, vol. 54, nos. 5–6, pp. 1584–1607, 2011.

[26] H. Zhou, P. Sun, and D. Zheng, "Practice-oriented intuitive approach for engineering undergraduates: A case study," *Int. J. Eng. Edu.*, vol. 28, no. 4, pp. 824–830, 2012.

[27] M. Demirtas, Y. Altun, and A. Istanbullu, "Virtual laboratory for sliding mode and PID control of rotary inverted pendulum," *Comput. Appl. Eng. Edu.*, vol. 21, no. 3, pp. 400–409, 2013.

[28] D. Qian, J. Yi, and D. Zhao, "How to automatically set an initial angle for balance control of a cart-pole system: An education case," *Int. J. Elect. Eng. Edu.*, vol. 50, no. 1, pp. 57–68, 2013.

[29] M. Canale and S. Casale-Brunet, "A multidisciplinary approach for model predictive control education: A lego mindstorms NXT-based framework," *Int. J. Control, Autom., Syst.*, vol. 12, no. 5, pp. 1030–1039, 2014.

[30] J. Lin, S. Y. Chen, and W.-H. Gau, "Design and implementation of a novel inertia flywheel pendulum mechatronic kit," *J. Vibrat. Control*, vol. 21, no. 16, pp. 3417–3430, 2015.

[31] B. Zupančič and A. Sodja, "Computer-aided physical multi-domain modelling: Some experiences from education and industrial applications," *Simul. Model. Pract. Theory*, vol. 33, pp. 45–67, Apr. 2013.

[32] O. Špinka, J. Åkesson, Z. Hanzálek, and K.-E. Årzén, "Open physical models in control engineering education," *Int. J. Elect. Eng. Edu.*, vol. 47, no. 4, pp. 448–459, 2010.

[33] J. H. Lee, H. J. Shin, S. J. Lee, and S. Jung, "Balancing control of a single-wheel inverted pendulum system using air blowers: Evolution of mechatronics capstone design," *Mechatronics*, vol. 23, no. 8, pp. 926–932, 2013.

[34] J. Roubal, P. Husek, and J. Stecha, "Linearization: Students forget the operating point," *IEEE Trans. Educ.*, vol. 53, no. 3, pp. 413–418, Aug. 2010.

[35] I. Fantoni and R. Lozano, "Stabilization of the Furuta pendulum around its homoclinic orbit," *Int. J. Control*, vol. 75, no. 6, pp. 390–398, 2002.

[36] I. Fantoni and R. Lozano, *Non-linear Control for Underactuated Mechanical Systems*. London, U.K.: Springer-Verlag, 2002.

[37] F. Gordillo, J. A. Acosta, and J. Aracil, "A new swing-up law for the Furuta pendulum," *Int. J. Control*, vol. 76, no. 8, pp. 836–844, 2003.

[38] Y. S. Lee, J. J. Oh, S. Y. Shim, H. Lim, and J. H. Seo, "Swing-up control for a rotary inverted pendulum with restricted rotation range," *J. Inst. Control, Robot. Syst.*, vol. 14, no. 6, pp. 548–553, 2008.

[39] J.-W. Kim and C.-Y. Oh, "Control of a rotary inverted pendulum system using brain emotional learning based intelligent controller," *J. Korean Soc. Manuf. Technol. Eng.*, vol. 22, no. 5, pp. 837–844, 2013.

[40] Y.-F. Chen and A.-C. Huang, "Adaptive control of rotary inverted pendulum system with time-varying uncertainties," *Nonlinear Dyn.*, vol. 76, no. 1, pp. 95–102, 2014.

[41] M. F. Hamza, H. J. Yap, and I. A. Choudhury, "Genetic algorithm and particle swarm optimization based cascade interval type 2 fuzzy PD controller for rotary inverted pendulum system," *Math. Problems Eng.*, vol. 2015, Art. no. 695965, May 2015. [Online]. Available: http://www.hindawi.com/journals/mpe/2015/695965/

[42] S.-K. Oh, W.-D. Kim, and W. Pedrycz, "Design of optimized cascade fuzzy controller based on differential evolution: Simulation studies and practical insights," *Eng. Appl. Artif. Intell.*, vol. 25, no. 3, pp. 520–532, 2012.

[43] P. Seman, B. Rohal'-Ilkiv, M. Juhás, and M. Salaj, "Swinging up the Furuta pendulum and its stabilization via model predictive control," *J. Elect. Eng.*, vol. 64, no. 3, pp. 152–158, 2013.

[44] J. Aracil, J. Á. Acosta, and F. Gordillo, "A nonlinear hybrid controller for swinging-up and stabilizing the Furuta pendulum," *Control Eng. Pract.*, vol. 21, no. 8, pp. 989–993, 2013.

[45] C.-C. Cheng, K.-S. Yang, and J.-H. Yang, "Robust finite time controller design for second order nonlinear underactuated mechanical systems," *Trans. Can. Soc. Mech. Eng.*, vol. 37, no. 3, pp. 549–557, 2013.

[46] M. Ramírez-Neria, H. Sira-Ramírez, R. Garrido-Moctezuma, and A. Luviano-Juárez, "Linear active disturbance rejection control of underactuated systems: The case of the Furuta pendulum," *ISA Trans.*, vol. 53, no. 4, pp. 920–928, 2014.

[47] C. Aguilar-Avelar and J. Moreno-Valenzuela, "A composite controller for trajectory tracking applied to the Furuta pendulum," *ISA Trans.*, vol. 57, pp. 286–294, Jul. 2015.

[48] A. S. Shiriaev, L. B. Freidovich, A. Robertsson, R. Johansson, and A. Sandberg, "Virtual-holonomic-constraints-based design of stable oscillations of Furuta pendulum: Theory and experiments," *IEEE Trans. Robot.*, vol. 23, no. 4, pp. 827–832, Aug. 2007.

[49] L. Freidovich, A. Shiriaev, F. Gordillo, F. Gomez-Estern, and J. Aracil, "Partial-energy-shaping control for orbital stabilization of high-frequency oscillations of the Furuta pendulum," *IEEE Trans. Control Syst. Technol.*, vol. 17, no. 4, pp. 853–858, Jul. 2009.

[50] L. T. Aguilar, I. Boiko, L. Fridman, and R. Iriarte, "Generating self-excited oscillations for underactuated mechanical systems via two-relay controller," *Int. J. Control*, vol. 82, no. 9, pp. 1678–1691, 2009.

[51] M. Fliess, J. Lévine, P. Martin, and P. Rouchon, "Flatness and defect of non-linear systems: Introductory theory and examples," *Int. J. Control*, vol. 61, no. 6, pp. 1327–1361, 1995.

[52] M. R. Rani, H. Selamat, H. Zamzuri, and Z. Ibrahim, "Multi-objective optimization for PID controller tuning using the global ranking genetic algorithm," *Int. J. Innov. Comput., Inf. Control*, vol. 8, no. 1, pp. 269–284, 2012.

[53] A. Ahmadi, H. A. Rahim, and R. A. Rahim, "Optimization of a self-tuning PID type fuzzy controller and a PID controller for an inverted pendulum," *J. Intell. Fuzzy Syst.*, vol. 26, no. 4, pp. 1987–1999, 2014.

[54] J.-X. Xu, Z.-Q. Guo, and T. H. Lee, "Synthesized design of a fuzzy logic controller for an underactuated unicycle," *Fuzzy Sets Syst.*, vol. 207, pp. 77–93, Nov. 2012.

[55] M. Fliess, H. Sira-Ramírez, and R. Márquez, "Regulation of non-minimum phase outputs: A flatness based approach," in *Perspectives in Control*, D. Normand-Cyrot, Ed. London, U.K.: Springer-Verlag, 1998.

[56] N. Faiz, S. K. Agrawal, and R. M. Murray, "Trajectory planning of differentially flat systems with dynamics and inequalities," *J. Guid., Control Dyn.*, vol. 24, no. 2, pp. 219–227, 2001.

[57] M. Fliess, R. Marquez, and H. Mounier, "An extension of predictive control, PID regulators and Smith predictors to some linear delay systems," *Int. J. Control*, vol. 75, no. 10, pp. 728–743, 2002.

[58] M. Fliess, H. Mounier, P. Rouchon, and J. Rudolph, "A distributed parameter approach to the control of a tubular reactor: A multivariable case," in *Proc. 37th Conf. Decision Control*, Tampa, FL, USA, 1998, pp. 439–442.

[59] H. Sira-Ramírez and S. K. Agrawal, *Differentially Flat Systems*. New York, NY, USA: Marcel Dekker, 2004.

[60] J. J. Slotine and W. Li, *Applied Nonlinear Control*. Englewood Cliffs, NJ, USA: Prentice-Hall, 1989.

**VICTOR MANUEL HERNÁNDEZ-GUZMÁN** was born in Querétaro, QRO, Mexico. He received the B.S. degree from the Instituto Tecnológico de Querétaro, Querétaro, in 1988, the M.S. degree from the Instituto Tecnológico de la Laguna, Torreón, COAH, Mexico, in 1991, and the Ph.D. degree from the Centro de Investigación y de Estudios Avanzados del Instituto Politécnico Nacional, Mexico City, Mexico, in 2003, all in electrical engineering.

He has been a Professor with the Universidad Autónoma de Querétaro, Querétaro, since 1995, where he teaches classical and nonlinear control. He has co-authored the book *Automatic Control: Design Theory, Prototype Construction, Modeling, Identification, and Experimental Tests* (in Spanish) (Mexico City, Mexico: Colección CIDETEC-IPN, 2013). He has authored over 40 papers in refereed journals. His research interests include control of mechatronic systems, mobile robots, and electromechanical systems. This includes control of different classes of ac electric motors when actuating on complex nonlinear mechanical loads. He has a particular interest in prototype construction to teach classical and nonlinear control techniques.

**MAYRA ANTONIO-CRUZ** received the B.S. degree in mechatronics from the Instituto Tecnológico de Reynosa, Tamaulipas, Mexico, in 2012, and the M.S. degree in computing technology from CIDETEC-IPN, Mexico City, Mexico, in 2015, where she is currently pursuing the Ph.D. degree with the Department of Mechatronics.

Her current research interests include the theory and application of automatic control in underactuated mechanical systems, and power electronic systems. She is also interested in the development of educational technology. During her academic trajectory, she received the Best Academic Performance Award in the cycle of schooling 2014–2015. She was awarded with the Distinction to Polytechnic Merit: Presea Lázaro Cádenas 2016, in the physical and mathematical sciences area at master level.

**RAMÓN SILVA-ORTIGOZA** received the B.S. degree in electronics from the Benemérita Universidad Autónoma de Puebla, Puebla, Mexico, in 1999, and the M.S. and Ph.D. degrees in electrical engineering (mechatronics) from the Centro de Investigación y de Estudios Avanzados del Instituto Politécnico Nacional, Mexico City, Mexico, in 2002 and 2006, respectively.

He has been a Researcher with the Department of Mechatronics, CIDETEC-IPN, since 2006, and belongs to SNI-CONACYT, Mexico. He has co-authored the book *Control Design Techniques in Power Electronics Devices* (London, U.K.: Springer-Verlag, 2006). He was an Editor of the book *Mechatronics* (in Spanish) (Mexico City, Mexico: Colección CIDETEC-IPN, 2010). He has recently co-authored the book *Automatic Control: Design Theory, Prototype Construction, Modeling, Identification and Experimental Tests* (in Spanish) (Mexico City, Mexico: Colección CIDETEC-IPN, 2013). He has authored over 40 papers in refereed journals. His research interests include mechatronic systems control, mobile robotics, control in power electronics, and the development of educational technology.